Monthly Notices of the ROYAL ASTRONOMICAL SOCIETY

Mon. Not. R. Astron. Soc. (2011) doi:10.1111/j.1365-2966.2011.18285.x

Understanding the faint red galaxy population using large-scale clustering measurements from SDSS DR7

Ashley J. Ross,* Rita Tojeiro and Will J. Percival

Institute of Cosmology & Gravitation, Dennis Sciama Building, University of Portsmouth, Portsmouth PO1 3FX

Accepted 2011 January 2. Received 2010 December 21; in original form 2010 October 7

ABSTRACT

We use data from the SDSS to investigate the evolution of the large-scale galaxy bias as a function of luminosity for red galaxies. We carefully consider correlation functions of galaxies selected from both photometric and spectroscopic data, and cross-correlations between them, to obtain multiple measurements of the large-scale bias. We find, for our most robust analyses, a strong increase in bias with luminosity for the most luminous galaxies, an intermediate regime where bias does not evolve strongly over a range of two magnitudes in galaxy luminosity, and no evidence for an upturn in bias for fainter red galaxies. Previous work has found an increase in bias to low luminosities that has been widely interpreted as being caused by a strong preference for red dwarf galaxies to be satellites in the most massive haloes. We can recover such an upturn in bias to faint luminosities if we push our measurements to small scales, and include galaxy clustering measurements along the line of sight, where we expect non-linear effects to be the strongest. The results that we expect to be most robust suggest that the low-luminosity population of red galaxies is not dominated by satellite galaxies occupying the most massive haloes.

Key words: galaxies: general – galaxies: haloes – galaxies: statistics.

1 INTRODUCTION

The evolution of dark matter can be accurately modelled within the Lambda Cold Dark Matter (ΛCDM) scenario, giving the number density of collapsed objects (e.g. dark matter haloes) of given mass as a function of redshift. In the widely accepted model of galaxy evolution, galaxies form within the gravitational potential wells of host dark matter haloes (White & Rees 1978). Thus, we can reduce the problem of modelling galaxy populations to one of working out the set of assumptions on how to relate luminous with dark matter. In fact, simple instructions can provide an excellent description of the observed clustering of galaxies in the near (see, e.g. Norberg et al. 2002; Zehavi et al. 2010) and in the more distant universe (see, e.g. Coil et al. 2006; McCracken et al. 2007).

In the galaxy formation framework, structure builds hierarchically, with smaller haloes being the first to collapse and merge together to build up larger haloes over time. Galaxies, as permanent residents of these haloes, must therefore also grow through merging, but the link between galaxy growth (in terms of stellar mass) and halo growth (in terms of dark matter mass) is far from direct. First, stellar mass in galaxies may also grow through the process of turning cold gas into stars, and secondly galaxy growth through merging is slower than halo growth – galaxies do not always merge when their host haloes do, and there is strong evidence that stellar mass may not be conserved during such a process (Conroy, Ho & White 2007; White et al. 2007).

There is a firmly established colour bimodality in the galaxy population seen at low redshift (e.g. Blanton et al. 2003), and this continues to earlier epochs (e.g, Bell et al. 2004). This striking separation of the galaxy population into a blue (star forming) and red (quiescent) clouds must therefore be an outcome of any galaxy evolution model. Understanding how these two populations evolve, and how galaxies go from one cloud to the other (i.e. what process quenches star formation), has been a long-standing quest in galaxy evolution, and one for which clustering studies have the potential of being particularly insightful.

The large-scale clustering strength of a particular population of galaxies is directly linked to the host dark matter halo mass (Bardeen et al. 1986; Cole & Kaiser 1989). Consequently, studying the clustering properties of a sample of galaxies, as well as its evolution with redshift, remains as one of the most powerful ways to constrain galaxy evolution. Many previous studies have investigated the clustering of galaxies as a function of their colour and luminosity (recent studies include, e.g. Willmer, da Costa & Pellegrini 1998; Norberg et al. 2002; Budavári et al. 2003; Madgwick et al. 2003; Zehavi et al. 2005; Croton et al. 2006; Ross, Brunner & Myers 2007; McCracken et al. 2008; Ross & Brunner 2009; Tinker & Wetzel 2010; Zehavi et al. 2010). In broad terms, it has become clear that the large-scale clustering strength increases with luminosity and with redder colour.

*E-mail: Ashley.Ross@port.ac.uk

© 2011 The Authors
Monthly Notices of the Royal Astronomical Society © 2011 RAS

Clustering measurements of galaxy subpopulations, in one sense, represent statistical restatements and refinements of the well known morphology–density relationship (Dressler 1980), which is now known more accurately as a colour–density relationship (see, e.g. Ball, Loveday & Brunner 2008; Skibba et al. 2009). We now know that the bimodality in the colours of galaxies extends to their large-scale clustering strengths, revealing that a halo-mass dependent effect is important in delineating blue from red galaxies. Essentially, the most luminous, most red galaxies occupy the highest peaks in the density fields, and for any particular luminosity, red galaxies are found to occupy higher peaks than their blue counterparts. This suggests red galaxies were the first to begin their hierarchical mass assembly – qualitatively consistent with the interpretation that they are red because they have used up/been stripped of their cold gas (see, e.g. Larson, Tinsley & Caldwell 1980; Cowie et al. 1996).

If we now focus on the clustering of red galaxies, there is interesting evidence that their large-scale clustering strength increases towards the faint end (see, e.g. Norberg et al. 2002; Zehavi et al. 2005; Swanson et al. 2008; Cresswell & Percival 2009). The natural interpretation is that faint red galaxies are predominantly satellite galaxies in large-mass haloes. This would further imply that red galaxies with luminosities $\sim L^*$ prefer less massive haloes than their brighter and fainter counterparts – qualitatively consistent with the picture of S0 galaxies occupying groups and luminous and dwarf red galaxies occupying clusters.

While it is uncontroversial that a significant percentage of faint red galaxies are satellites in large-mass haloes, the exact proportion that are satellites, and whether this is sufficient that these galaxies dominate the population, is less clear. Wang et al. (2009), selecting on colour, find that dwarf red galaxies (fainter than those studied in any of the other cited works here) are predominantly central, rather than satellite galaxies. This is in contrast to Haines et al. (2007), who, when selecting on Hα emission, find nearly all red dwarf galaxies are satellites. Furthermore, there is some tension between analyses of large-scale bias and the work of Masjedi, Hogg & Blanton (2008), as they find that faint red galaxies have a very weak contribution of the growth of luminous red galaxies (LRGs), i.e. if the faint galaxies occupy the same haloes as LRGs, they are somehow precluded from merging with them. Finally, Brown et al. (2008) do not see an upturn in the large-scale bias towards fainter luminosities when studying red galaxies in the Bootes field, using photometric redshifts.

Motivated partly by the tension described in the previous paragraph, and partly by the desire to study fainter red galaxies, in this work we take a new look at the large-scale bias of red galaxies in the SDSS seventh and final data release, using both photometric and spectroscopic data. The photometric data allow us to analyse a significantly larger volume of the Universe containing the lower luminosity galaxies than the spectroscopic data. This means we can consider the same volume to analyse a wide range of galaxy luminosities. We also use the cross-correlation between these data with brighter spectroscopic data to confirm the robustness of our results.

This paper is organized as follows. In Section 2 we describe the photometric and spectroscopic redshift catalogues we use for our measurements. In Section 3 we describe how we measure correlation functions (angular auto- and cross-correlation functions and redshift space 3D auto-correlation functions) and how we use these measurements to measure the bias of galaxy samples. In Section 4, we present the bias measurements from our photometric redshift samples, and in Section 5 from our spectroscopic redshift samples. In Section 6, we compare our spectroscopic and photometric results to each other and to the results of previous studies. In Section 7, we discuss the physical implications of our measurements and in Section 8, we present a summary of our conclusions.

Throughout, we use M_r as shorthand for $M_r - 5\log(h)$. We assume a flat cosmology with $\Omega_{\rm m} = 0.25$, $h = 0.7$, $\sigma_8 = 0.8$ and $\Omega_{\rm b} = 0.045$.

2 DATA

We use data from the SDSS seventh data release (DR7). This survey obtained wide-field CCD photometry (Gunn et al. 1998) in five passbands (u, g, r, i, z; e.g. Fukugita et al. 1996), amassing nearly 10 000 deg^2 of imaging data for which object detection is reliable to $r \sim 22$ (Abazajian et al. 2009). From these photometric data, spectroscopic targets have been identified and observed yielding a sample of galaxies with over 600 000 spectroscopic redshifts complete to a Petrosian (1976) magnitude limit of $r < 17.77$ occupying over 8000 deg^2 (Abazajian et al. 2009). We utilize data from both the spectroscopic redshift catalogue (as this allows precise redshift information) and a photometric redshift catalogue (as this allows us to go more than 2 mag deeper).

The photometric redshifts used were obtained from the SDSS photoz table. Redshifts in this catalogue were estimated using a hybrid template/empirical approach, and the output includes rest-frame absolute magnitudes, k-corrections and galaxy-type values. We include all galaxies with $z_{\rm phot} < 0.1$ and $M_r < -17.75$ (which makes our sample approximately volume limited for $r < 20$). In order to select red galaxies, we use the (k-corrected) double colour cut

$$u - r > 2.2\,, \quad g - r > 0.8, \tag{1}$$

which ensures that the galaxies are truly red and there are few blue interlopers in our sample. Fig. 1 displays the distribution of $u - r$ colours of the galaxies in our red sample, with a solid line. The dashed displays the distribution we would have had if we simply selected $u - r > 2.2$. Our double cut clearly removes galaxies that are close to our cut limit, giving us a distinct sample of galaxies

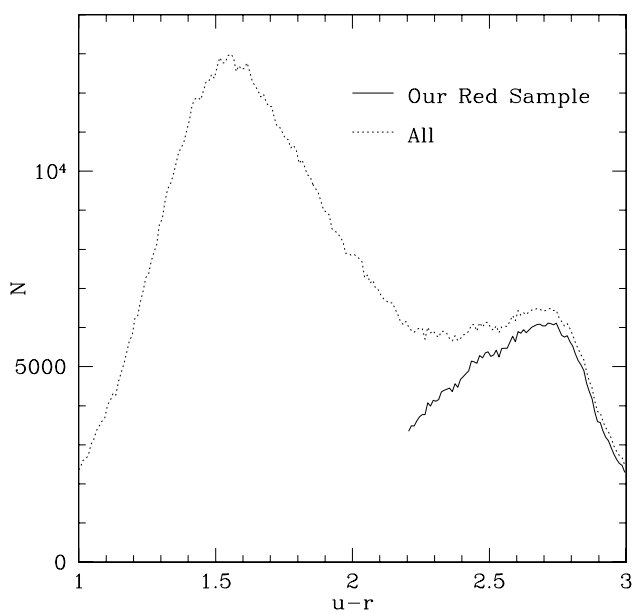

Figure 1. The distribution of $u - r$ colours of galaxies with $z_{\rm phot} < 0.1$ and $M_r < -17.75$ (dotted line) and for galaxies with only $u - r > 2.2$ and $g - r > 0.8$ (solid line).

© 2011 The Authors
Monthly Notices of the Royal Astronomical Society © 2011 RAS

(more so than selecting on type value provided in the photoz table). We find that performing this double cut also improves the reliability of the photometric redshift estimates. We further cut the data to the angular mask of Ross, Percival & Brunner (2010, hereafter R10), leaving just over 6000 deg^2 of observing area in the northern contiguous area of SDSS, and subdivide this sample into three subsamples with $-17.75 < M_r < -18.75$ (27 023 galaxies), $-18.75 < M_r < -19.75$ (23 081 galaxies) and $-19.75 < M_r < -20.75$ (17 156 galaxies).

We also consider galaxies selected from the main SDSS spectroscopic sample. The red galaxy samples were selected using the colour cut as defined by equation (1), dividing into five subsamples, by absolute magnitude, $-17 < M_r < -18$ (2082 galaxies), $-18 < M_r < -19$ (11 663 galaxies), $-19 < M_r < -20$ (54 908 galaxies), $-20 < M_r < -21$ (118 853 galaxies) and $-21 < M_r < -22$ (97 947 galaxies). Note that we place no redshift limits on the red spectroscopic galaxy samples we use.

We also consider spectroscopic samples without colour selection to cross-correlate against the photometric redshift samples. These samples were selected to be approximately volume limited; one is limited to $z < 0.15$, $M_r < -20.75$ (129 435 galaxies) and a second limited to $z < 0.1$, $M_r < -19.75$ (140 341 galaxies).

3 METHODOLOGY

We now outline the methodology used to calculate the bias of red galaxies as a function of their absolute magnitude. For the photometric data and for cross-correlations with the spectroscopic data, we use the projected angular correlation function. For the spectroscopic data we consider the full 3D correlation function.

3.1 Calculating angular correlation functions

In order to calculate angular auto-correlation and cross-correlation functions, $w(\theta)$, we use the Landy & Szalay (1993) estimator

$$w(\theta) = \frac{D_1 D_2(\theta) - D_1 R_2(\theta) - D_2 R_1(\theta) + R_1 R_2(\theta)}{R_2 R_2(\theta)}, \tag{2}$$

where D_1 and D_2 (and R_1 and R_2) represent separate data samples for the cross-correlation and are the same for the auto-correlation. Our random catalogue representing the photometric data contains 10 million points and is the same as used in R10. The photometric catalogues (data and random) are masked for seeing, reddening, bright stars, satellite trails, etc. in the same manner as R10. At scales larger than 1°, we employ a pixel based routine using SDSSpix. We use the pixel resolution (64) such that the pixels have an area with equivalent circular radius of 0°.083. We confirm that the point to point and pixelized methods agree at overlapping scales. The random catalogue representing the spectroscopic data contains over 6 million points and was created as described in (Reid et al. 2009), with a pixel based mask based on HEALPIX (Górski et al. 2005).

We use a jackknife method (e.g. Scranton et al. 2002), with inverse-variance weighting to estimate the errors and covariance matrix (e.g. Myers et al. 2007) for $w(\theta)$. The method is nearly identical to the method described in detail in Ross et al. (2007, hereafter R07) and applied to DR7 data in R10. The jackknife method works by creating many subsamples of the entire data set, each with a small part of the total area removed. R07 found that 20 jack-knife subsamplings are sufficient to create a stable covariance matrix, and we therefore use 20. These 20 subsamples are created by extracting a contiguous grouping of 1/20th of the unmasked pixels in 20 separate areas. Our covariance matrix, C_w, is thus given by

$$\begin{aligned} C_{i,j,w} &= C_w(\theta_i, \theta_j) \\ &= \frac{19}{20} \sum_{k=1}^{20} [\omega_{\rm full}(\theta_i) - \omega_k(\theta_i)][\omega_{\rm full}(\theta_j) - \omega_k(\theta_j)], \end{aligned} \tag{3}$$

where $\omega_k(\theta)$ is the value for the correlation measurement omitting the kth subsample of data and i and j refer to the ith and jth angular bin. The jackknife errors are simply the square-root of diagonal elements of the covariance matrix.

3.2 Calculating 3D correlation functions

In order to calculate the 3D auto-correlation function, $\xi(r, \mu)$, we again employ the Landy & Szalay (1993) estimator but in this case DD, DR and RR are now functions of r, the physical separation we calculate given our assumed cosmology, and also μ, the cosine of the angle between the radial direction and the alignment of a galaxy pair. Further, we must assign the random points radial positions, which we do by sampling a fine resolution cubic spline fit to the galaxy redshift distribution. We also weight each galaxy according to the number density at its radial position (Feldman, Kaiser & Peacock 1994): this weight is optimal if the galaxies Poisson sample the density field.

We analytically estimate the errors and covariance of the $\xi(r, \mu)$ measurements. Given optimal weights, $w(r) = 1/(1 + \bar{n}(r)P(k))$, and the power spectrum, $P(k)$, its error can be estimated by (Tegmark 1997)

$$\sigma_{\rm p}^2(k) = \frac{(2\pi)^3 P(k)^2}{V_k V_{\rm eff}(k)}, \tag{4}$$

where $V_{\rm eff}(k) = \int [\frac{\bar{n}(r)P(k)}{1+\bar{n}(r)P(k)}]^2 {\rm d}^3 r$ and $V_k = 4\pi k^2 \Delta k$. Given that the correlation function is just the Fourier transform of the power spectrum, we can estimate the covariance, C_ξ, in the measured ξ between bins centred at r_1 and r_2 as

$$C_\xi(r_1, r_2) = \frac{1}{2\pi^2} \int \frac{{\rm d}k\, P(k)^2 \sin(r_1 k) \sin(r_2 k)}{r_1 r_2 V_{\rm eff}(k)} + \delta_{r_1, r_2}/n_{\rm p}, \tag{5}$$

where δ is the Kronecker delta, and $n_{\rm p}$ is the number of pairs included in the bin. Note that although this procedure ignores correlations induced by the sample window function, it should be sufficiently accurate for the analysis attempted in this work, as we only wish to measure the broad amplitude of the clustering rather than the relative clustering on different scales; for such measurements of amplitude, correlations between data are unimportant.

3.3 Theoretical modelling

We model the non-linear power-spectrum using the fitting formulae of Smith et al. (2003), which we use in combination with the transfer function of Eisenstein & Hu (1998) to include the effects of baryons. Given this power-spectrum, we determine the isotropic 3D real-space correlation function $\xi(r)$ via Fourier transform. We model the redshift-space correlation function as (Hamilton 1992)

$$\xi^s(\mu, r) = \xi_o(r) P_o(\mu) + \xi_2(r) P_2(\mu) + \xi_4(r) P_4(\mu), \tag{6}$$

where

$$\xi_0(r) = \left(b^2 + \frac{2}{3} bf + \frac{1}{5} f^2\right) \xi(r), \tag{7}$$

$$\xi_2(r) = \left(\frac{4}{3} bf + \frac{4}{7} f^2\right) [\xi(r) - \xi'(r)], \tag{8}$$

© 2011 The Authors
Monthly Notices of the Royal Astronomical Society © 2011 RAS

$$\xi_4(r) = \frac{8}{35} f^2 \left[\xi(r) + \frac{5}{2}\xi'(r) - \frac{7}{2}\xi''(r) \right], \quad (9)$$

P_ℓ are the standard Legendre polynomials, and

$$\xi' \equiv 3r^{-3} \int_0^r \xi(r')(r')^2 \mathrm{d}r' \quad (10)$$

$$\xi'' \equiv 5r^{-5} \int_0^r \xi(r')(r')^4 \, \mathrm{d}r', \quad (11)$$

b is the large-scale bias of the galaxy population being considered. We will be comparing our models to measurements limited to different maximum μ values. Thus, the model will become

$$\xi^s(\mu_{\max}, r) = \int_0^{\mu_{\max}} \xi^s(\mu, r) \mathrm{d}\mu / \mu_{\max} \quad (12)$$

In order to calculate model $w(\theta)$, we must project $\xi^s(\mu, r)$ over the radial distribution of galaxy pairs in a particular sample (or samples in the case of cross-correlations).

$$w(\theta) = \int \mathrm{d}z_1 \int \mathrm{d}z_2 n_i(z_1) n_j(z_2) \xi^s \left[\mu, r(\theta, z_1, z_2)\right], \quad (13)$$

where n_i is the normalized redshift distribution of sample i (and $i = j$ for the auto-correlation). The galaxy separation r is a function of the angular separation of the galaxies θ and their redshifts z_1 and z_2 (as is μ).

3.4 Modelling redshift distributions

The photometric redshifts we use have significant error associated with each redshift estimate. This implies that estimation of the true redshift distribution of the photometric redshift data is not trivial. In order to estimate the true redshift distribution for each of our photometric samples, we follow the procedure outlined in R10. Given a redshift estimate and its error, we assume a Gaussian PDF. We then convolve this PDF with the luminosity function and volume element/redshift relationship to obtain a final PDF, which we then sample 10 times. In this work, we find that adding a bias to the photometric redshifts (simply a shift in the mean) of +0.005 for each sample allows for the best agreement between all of our clustering measurements (see Section 4).

We can construct M_r distributions in a similar manner. Given the M_r of the redshift estimate, we can calculate the value of M_r at any point along the redshift PDF based on the change in the distance modulus, thus obtaining a PDF of M_r for each galaxy. This allows us to determine the expected mean M_r for any particular photometric redshift sample. When we calculate angular cross-correlations between photometric and spectroscopic samples, the redshift ranges of the samples are not matched. Thus, the distribution of luminosities of the galaxies that contribute to the measured clustering signal will not necessarily match that of either sample. In order to find the expected mean M_r of galaxies contributing to the cross-correlation, we can simply ignore the parts of the redshift PDF outside the spectroscopic redshift bound and thereby determine the effective mean M_r of photometric galaxies between any chosen spectroscopic redshift bounds.

3.5 Calculating bias values

We assume a simple linear bias model between the the two-point clustering in the dark matter and galaxy overdensity fields, such that the bias b, is defined by

$$P(k)_{\mathrm{g}} = b^2 P(k)_{\mathrm{DM}}. \quad (14)$$

In the regime where linear theory is a good approximation this relationship naturally extends to $\xi(r)$ and $w(\theta)$. The use of the Smith et al. (2003) non-linear $P(k)$ has the potential to extend this relationship to weakly non-linear scales. Thus, for arbitrary limits (but always assuming b is scale independent in equation 14) we determine the best-fitting value of b for a particular galaxy sample by minimizing

$$\chi^2 = \sum_{i,j} \left[w(\theta_i) - \hat{w}(\theta_i)\right] C_w^{-1}(\theta_i, \theta_j) [w(\theta_j) - \hat{w}(\theta_j)], \quad (15)$$

where the model correlation function $\hat{w}$ and χ^2 are implicitly dependent on the value of b. For the 3D correlation functions, $w(\theta)$ is replaced by $\xi^s(r, \mu_{\max})$ and θ by r.

4 BIAS FROM PHOTOMETRIC DATA

We measure the bias of galaxies in our photometric samples by measuring their respective auto-correlations and cross-correlations with the spectroscopic sample of galaxies with $z_{\mathrm{spec}} < 0.15$ and $M_r < -20.75$ (which we denote 'full'). The redshift limit means this sample covers most of the redshift distribution of the photometric samples and the absolute magnitude limit ensures that the bias of the galaxies in the sample should not change significantly with redshift. Based on $w(\theta)$ measurements with $\theta > 1^\circ$, the bias of the full spectroscopic sample is 1.32 ± 0.04, which agrees with the results of Zehavi et al. (2010), as it lies between the bias values of their $M_r < -20.5$ and $M_r < -21$ samples.

We determine the mean M_r of each photometric sample by estimating the distribution of M_r values as described in Section 3.4. The cross-correlation with the spectroscopic sample implies a hard limit of $z < 0.15$ for the photometric galaxies contributing signal to the measured cross-correlations. We find that imposing this limit when calculating the magnitude distribution changes the mean M_r value by less than 0.05 mag in every case. This implies that the $z < 0.15$ limit makes only a small difference to any of the magnitude distributions of the photometric galaxies that contribute to the cross-correlation signal. Therefore, it is valid to expect the bias of the photometric galaxies contributing to the auto-correlation signal to be the same as the bias of the photometric galaxies contributing signal to the cross-correlation with the $z < 0.15$ spectroscopic sample.

Fig. 2 displays the measured $w(\theta)$ for our three main photometric samples. The auto-correlations are shown by the black triangles and the cross-correlations are displayed in red squares, with luminosity increasing from bottom to top. The solid curves display the best-fitting model $w(\theta)$ fit for $1^\circ < \theta < 5^\circ$, where we have jointly fit the $w(\theta)$ auto- and cross-correlations (note, bias values can be independently determined for the auto- and cross-correlations; the joint-fit determines the most consistent value and reduces the overall uncertainty). We restrict the fits to $\theta < 5^\circ$ because systematic effects in the data (due to, e.g. reddening and star/galaxy separation) and the modelling [effects of redshift space distortions (RSD)] become more significant at larger angular scales. The jack-knife errors increase only slightly over our range of measurements, due to competing effects of cosmic variance and shot noise. The mean M_r and best-fitting b values corresponding to these joint fits are -18.46, 1.2 ± 0.05, -19.46, 1.43 ± 0.07, and -20.39, 1.40 ± 0.07, with respective χ^2 values of 13.3, 16.0 and 17.0 [and 13 degrees of freedom (d.o.f.)]. We note that these values remain constant (within the 1σ error-bars) regardless of the minimum scale we fit to between $0^\circ.5$ and $2^\circ.0$.

© 2011 The Authors
Monthly Notices of the Royal Astronomical Society © 2011 RAS

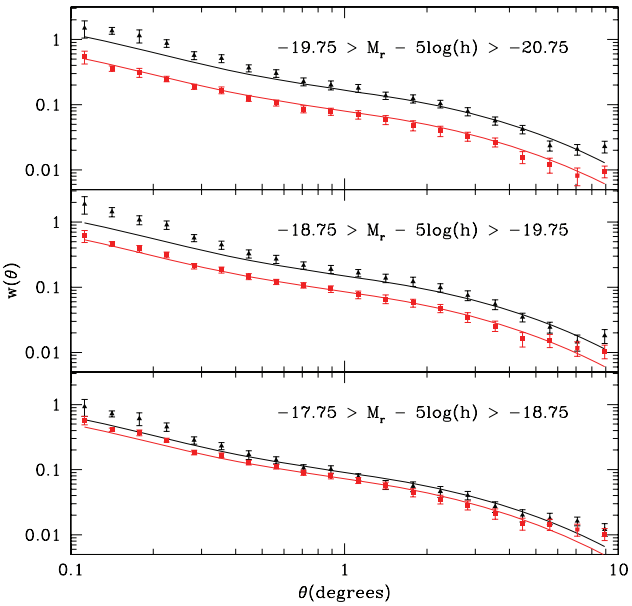

Figure 2. The measured angular auto-correlations for the three specified photometric samples, all with $z_{\rm phot} < 0.1$ (black triangles) and their cross-correlations (red squares) with the spectroscopic sample with $z < 0.15, M_r < -21.75$. The black and red curves display the respective best-fitting models (all fit between 1°.0 and 5°.0).

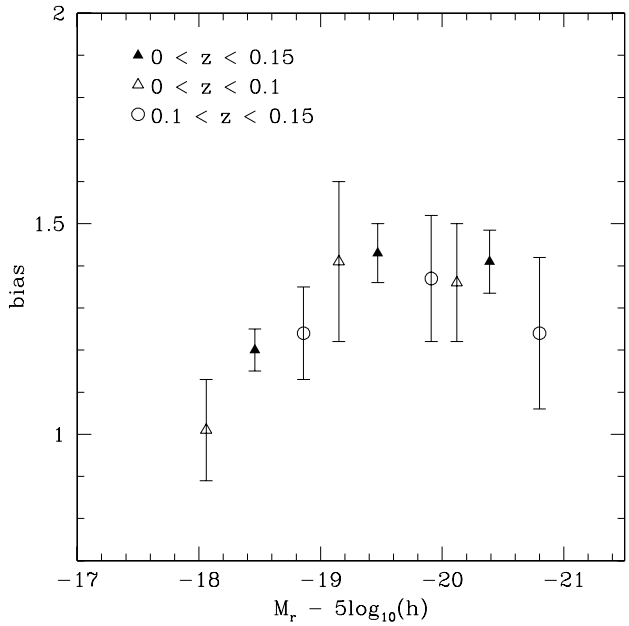

Figure 3. The measured bias values using the combination of the photometric auto-correlation and the cross-correlations with the $z_{\rm spec} < 0.15$, $M_r < -20.75$ sample (solid triangles), the cross-correlation with the $z_{\rm spec} < 0.1$, $M_r < -19.75$ ('near', open triangles), and the cross-correlation with the $0.1 < z_{\rm spec} < 0.15$, $M_r < -20.75$ data ('far', open circles).

In order to test the robustness of these results to the photometric redshift determination, we have also obtained estimates of b for galaxies of different luminosity by cross-correlating the photometric samples with spectroscopic samples covering different redshift ranges. The cross-correlation signal depends on the number of galaxies in the photometric sample that lie within the redshift range covered by the spectroscopic sample, so testing whether these bias estimates match those from our full sample tests the assumed distribution of photometric redshifts. We cross-correlate each photometric sample with two additional spectroscopic samples; one with $z < 0.1, M_r < -19.75$ (which denote 'near') and second with $0.1 < z < 0.15, M_r < -20.75$ (which we denote 'far'). We find that these redshift limits increase/decrease the mean value of M_r of the galaxies contributing to the cross-correlation signal by ∼0.4 mag. We find the bias of the near sample is 1.17 ± 0.05 (again in agreement with Zehavi et al. 2010) and we continue to use $b = 1.32 \pm 0.04$ for the far sample. Note that the near and far bias values can be determined only from the cross-correlations, since auto-correlations of the photometric data cannot replicate the effects of a hard redshift cut.

We display the best-fitting b against M_r for galaxies in our photometric redshift samples in Fig. 3. Values determined from the near cross-correlation are shown by the open triangles, while values determined from the far cross-correlation are shown by the open circles. The b values determined from the joint fit to the photometric auto- and cross-correlations with the full spectroscopic sample are plotted with solid triangles. Note that the joint fit estimates of b serve as our primary results, while the additional cross-correlations serve as a (correlated) consistency check.

The fact that the results from all cross-correlations agree is important confirmation that photometric redshift distributions we have estimated are accurate. We note that if we do not include the photometric redshift bias of +0.005, the cross-correlations do not yield consistent results. For every sample, the cross-correlation with the near data would imply a much lower (by ∼30 per cent) value of b and the cross-correlation with the far sample would yield a much higher (by ∼25 per cent) value of b, implying (the obviously incorrect result) that $b(M_r)$ would be highly oscillatory. However, this photometric redshift bias does not have a strong effect on the best-fitting b values of the three main samples. When the photometric redshift bias is set to zero, the best-fitting b values decrease slightly to 1.19 ± 0.05, 1.39 ± 0.07 and 1.38 ± 0.07 with increasing luminosity.

We have tested our results further by making changes both to the data we use and the modelling. We find that our results do not change (within 1σ) regardless of the minimum angular scale we use to find the best-fitting data. We have investigated multiplying the error on the photometric redshifts by a constant factor and leaving this parameter free when finding the best-fitting model. We find that this can slightly improve the χ^2 values, but not to the extent demanded by removing a degree of freedom. Importantly, doing so does not change the trend we find with M_r – the bias of the lowest luminosity red galaxies is always lowest. We find the same behaviour with different colour cuts and also if we make changes to the redshift/magnitude limits. No matter the analysis we apply, we find the same result – red galaxies with $M_r > -19$ have lower bias than their brighter counterparts. The bias measurements of the photometric galaxies thus suggest that the bias of red galaxies is approximately constant between $-19 > M_r > 21$ and decreases to lower luminosities.

5 BIAS FROM SPECTROSCOPIC DATA

We measure $\xi^s(\mu < \mu_{\rm max}, r)$ in order to determine best-fitting values of b for the five different spectroscopic samples of red galaxies with magnitudes between −17 and −22. The results of these measurements, for $\mu_{\rm max} = 1$ (bottom) and for $\mu_{\rm max} = 0.5$ (top) are displayed in Fig. 4. The two most luminous samples ($-21 < M_r < -22$,

© 2011 The Authors
Monthly Notices of the Royal Astronomical Society © 2011 RAS

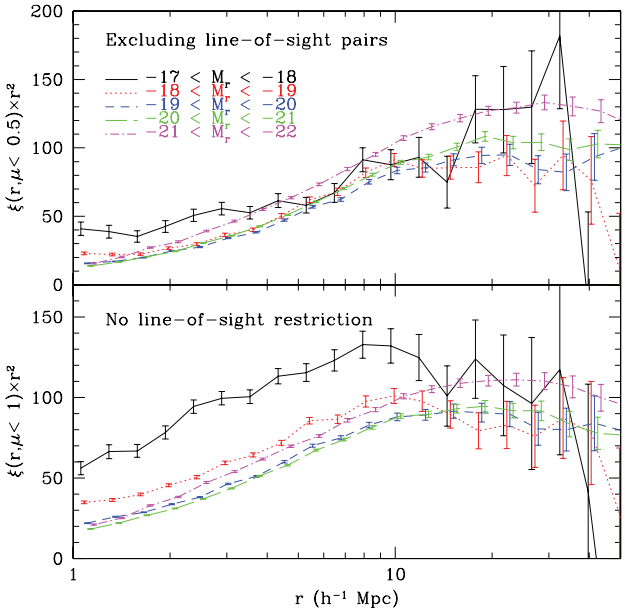

Figure 4. The measured redshift-space correlation function multiplied by r^2 for the five spectroscopic samples: $-17 < M_r < -18$ (black), $-18 < M_r - 19$ (red), $-19 < M_r - 20$ (blue), $-20 < M_r < -21$ (green) and $-21 < M_r < -22$ (magenta). The top panel displays the measurements when we restrict $\mu < 0.5$ and the bottom panel displays the results with no such restrictions.

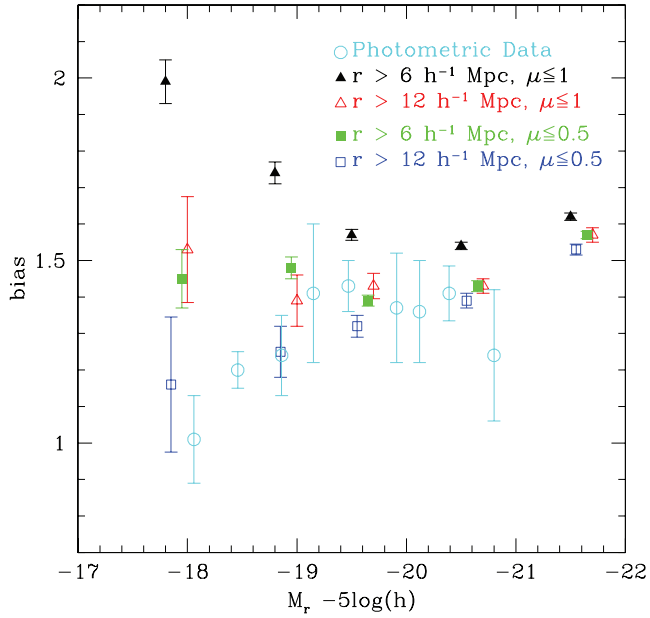

Figure 5. The measured bias of red spectroscopic galaxies as a function of M_r, for four different choices of $r_{\rm min}$ and $\mu_{\rm max}$. The M_r values have each been shifted slightly for clarity. For comparison, the bias values of the red photometric galaxies (same as plotted in Fig. 3) are displayed with cyan open circles.

magenta; $-20 < M_r < -21$, green) display smooth shapes over the range of the plot and are consistent with respect to each other for both $\mu_{\rm max}$ values. The least-luminous bin ($-17 < M_r < -18$) is quite noisy and displays a dramatic difference when $\mu_{\rm max}$ is changed – its clustering amplitudes are roughly double those of the most luminous sample for $r < 10\,h^{-1}$ Mpc when $\mu_{\rm max} = 1$ but this behaviour is removed for $\mu_{\rm max} = 0.5$. The two samples $-18 < M_r - 19$ (red) and $-19 < M_r < -20$ also display significant dependence on the scale and $\mu_{\rm max}$, as both display (relatively) larger amplitudes at smaller scales and greater $\mu_{\rm max}$ values. We note, however, that any cut that is more restrictive than $\mu < 0.5$ does not produce a statistically significant change in any of our bias measurements.

Not surprisingly, we find there is a strong dependence both on the minimum r and maximum μ that we use when we estimate b for the spectroscopic samples. Fig. 5 plots b versus M_r for four separate $r_{\rm min}/\mu_{\rm max}$ limits. For all bias estimates, the maximum scale we fit to is $40\,h^{-1}$ Mpc. If we use all angles to the line of sight and fit above $6\,h^{-1}$ Mpc (black triangles), we find that the bias increases as the luminosity of the red galaxies decreases. This behaviour is similar to that reported previously by Swanson et al. (2008) and also Cresswell & Percival (2009). However, if we fit for $r_{\rm min} > 12\,h^{-1}$ Mpc (open red triangles) or $\mu < 0.5$ (green squares), we see only weak evidence of an increase in the bias towards lower luminosity. If we require both that $r_{\rm min} > 12\,h^{-1}$ and $\mu < 0.5$ (open blue squares), we recover a monotonic increase in the bias with luminosity. The best-fitting bias values for $r > 12\,h^{-1}$ Mpc and $\mu \leq 0.5$ are consistent with the trend we found in the photometric data (plotted in Fig. 5 with open cyan circles).

The bias results that we expect to have the least systematic effects are those calculated from measurements at the largest scales (since we expect linear theory to be most valid at larger physical scales) and those calculated for pairs furthest from the line of sight, since they should be the least dependent on RSD. Note that we minimize the effects of linear RSD. We do allow for linear RSD in our modelling, but studies (see, e.g. Percival & White 2009; Jennings, Baugh & Pascoli 2011) have shown that linear RSD models begin to fail at larger scales than real-space clustering models. Perhaps more importantly, we minimize any of Fingers-of-God (FoG) effects (Jackson 1972). The effects of FoG imply that, by restricting our analysis to transverse pairs, we are preferentially discounting pairs of galaxies within dark-matter haloes. Note that for the purposes of measuring the linear bias, this is entirely appropriate, as the clustering of galaxies within dark matter haloes is clearly non-linear.

We thus believe that, of the data included in Fig. 5, the $r > 12\,h^{-1}$ Mpc, $\mu \leq 0.5$ results are the most trustworthy. The χ^2/d.o.f. values are all much smaller for the $r > 12\,h^{-1}$ Mpc fits, as for $\mu \leq 1$, the χ^2/d.o.f. values are all greater (and as high as 6) than 2.4 for $r > 6\,h^{-1}$ Mpc and they are all less than 1 for $r > 12\,h^{-1}$ Mpc. For $\mu \leq 0.5$, the difference is not as extreme, but in every case the χ^2/d.o.f. values are reduced when the fit is performed at larger scales. For the faintest bin, the bias we measure is sensitive to the particular $\mu_{\rm max}$, $r_{\rm min}$ we choose (it continues to vary significantly if we increase $r_{\rm min}$ beyond $12\,h^{-1}$ Mpc), suggesting that the systematic error associated with this bias measurement is much larger than the statistical error displayed in Fig. 5 and subsequent figures.

6 COMPARISON TO PREVIOUS RESULTS

Our most robust results suggest there is monotonic *increase* in the bias of red galaxies with luminosity between $-17.5 > M_r > -19.5$. This disagrees with recent findings. A comparison between a selection of our results for the spectroscopic data compared to some previously published results is displayed in Fig. 6. We have normalized the bias values of previous studies such that the bias of red galaxies with magnitudes closest to $M_r = -20.5$ is equal to 1.4. For the Zehavi et al. (2010) results, we have used the $w_{\rm p}(r_{\rm p})$ measurements they list in table B9 at scales $6 < r_{\rm p} < 17\,h^{-1}$ Mpc. We simply determine the inverse-variance weighted mean of the

© 2011 The Authors
Monthly Notices of the Royal Astronomical Society © 2011 RAS

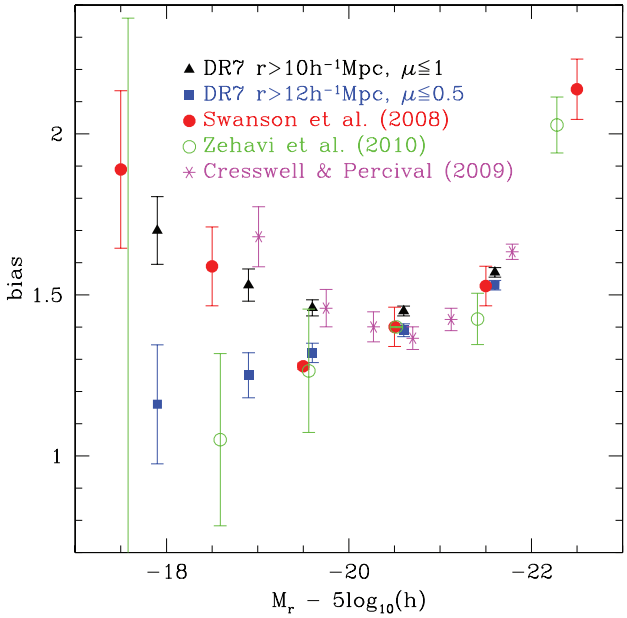

Figure 6. The measured bias of red spectroscopic galaxies as a function of M_r, for $r > 10\,h^{-1}$ Mpc, $\mu_{\max} = 1$ and $r > 12\,h^{-1}$ Mpc, $\mu_{\max} = 0.5$. Also plotted are the recent results of three other recent studies of the clustering of red galaxies.

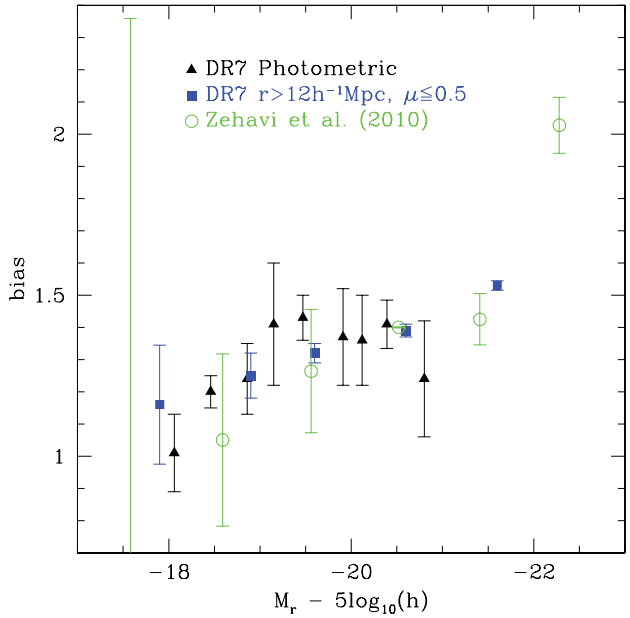

Figure 7. The measured bias of red galaxies, considering only DR7 measurements with minimal contribution from pairs along the line of sight.

ratio between each of their samples and the $-20 > M_r > -21$ sample and then take its square root to estimate the relative bias of each of their samples.

All of the results plotted in Fig. 6 agree quite well for galaxies with $M_r < -20$. In fact, for $M_r < -19$, the agreement between our spectroscopic analysis with $r_{\min} = 12\,h^{-1}$ Mpc, $\mu_{\max} = 0.5$ (blue squares), Swanson et al. (2008) and Zehavi et al. (2010) is excellent. For less luminous galaxies, the bias is strongly dependent on the sample and method used. We find that a choice of $r_{\min} = 10\,h^{-1}$ Mpc, $\mu_{\max} = 1$ (black triangles) for the spectroscopic data analysis produces a result that is quite similar to Cresswell & Percival (2009) and Swanson et al. (2008), while the fit with $r_{\min} = 12\,h^{-1}$ Mpc, $\mu_{\max} = 0.5$ (blue squares) shows strong disagreement.

The dramatic change in the best-fitting bias as a function of $r_{\min}$ and $\mu_{\max}$ suggests that non-linear effects have a great influence on the clustering of faint red galaxies, even to scales $\sim 10\,h^{-1}$ Mpc. The correlation function measurements we perform on the spectroscopic samples (see Fig. 4) are consistent with the results of Hogg et al. (2003) and Blanton et al. (2005), which found bright and faint red galaxies to have the highest overdensities on $8\,h^{-1}$ Mpc scales. Cresswell & Percival (2009) fit their power spectra measurements to similarly small scales, as they used $k < 0.21\ h\,\mathrm{Mpc}^{-1}$. Further, the measurements of Norberg et al. (2002) were restricted to $r < 5\,h^{-1}$ Mpc, and their bias estimates are therefore quite different than ours. Larger scales appear to be required in order to escape the influence of non-linearities. Swanson et al. (2008) use a larger physical scale ($20\,h^{-1}$ Mpc) for the radius of their cells, but being that they use counts-in-cells, the counts in large cells are highly covariant with those of smaller scales, and non-linearities may persist. Further, while all of the studies we cite do attempt to account for RSD, none explicitly remove pairs oriented along the line of sight, suggesting the possibility that systematic effects may still be present.

If we focus only on DR7 data with minimal contribution from clustering along the line of sight, the result is shown in Fig. 7 [the $w_{\rm p}(r_{\rm p})$ and $w(\theta)$ measurements should be dominated by transverse pairs]. Within the 1σ error-bars, only the measured bias of the $M_r \sim -19.5$ photometric sample appears inconsistent with the rest of the data, but it is consistent to within 2σ. Given the number of data points (19), this is reasonable statistically. The consistency of the data can be further confirmed by the fact that a fit to $b(M_r) = (a(M_r + 20))^3 + b_o$ has minimum $\chi^2 = 7.2$ for $a = -0.35$ and $b_o = 1.36$ (this suggests only that this data is consistent with a smoothly varying function and we do not believe it should be extrapolated outside of the M_r values we present). The combination of data suggests that the bias of red galaxies increases dramatically for galaxies more luminous than -21.5, the bias of red galaxies is nearly constant for $-19 > M_r > -21$, but for $M_r > -19$ the bias decreases significantly.

A reasonable interpretation of the compiled results is that the previously reported increase in the bias of red galaxies as the luminosity decreases is correct only for non-linear scales and therefore has no relation to the average mass of the haloes that faint red galaxies occupy. Non-linear effects were made stronger due to redshift distortions and non-linear clustering, further exacerbated by the very small volume occupied by the low luminosity galaxies. The studies that utilize larger volumes (the photometric data) or use results only where the influence of clustering along the line of sight is minimized (the spectroscopic data herein with $\mu < 0.5$, Li et al. 2006; Zehavi et al. 2010) agree that the bias of red galaxies displays a monotonic increase with luminosity.

7 PHYSICAL INTERPRETATION

Our results suggest that redshift distortions and non-linear clustering have a large effect on the measured clustering of faint red galaxies, even at large scales. Physically, this makes sense. We know that a significant percentage of faint red galaxies are satellites in high-mass haloes. This implies that a significant proportion of the pairs of faint red galaxies are satellites within the same dark matter halo and their true physical separations are as large as a few h^{-1} Mpc (the Virial radius of a $10^{14}\,\mathrm{M}_\odot\,h^{-1}$ halo is $\sim 1\,h^{-1}$ Mpc). Thus, even

© 2011 The Authors
Monthly Notices of the Royal Astronomical Society © 2011 RAS

given the true 3D distribution of galaxies, we would expect to find non-linear effects have more influence on the clustering of faint red galaxies than for other galaxy sub-populations.

Finger-of-God effects exacerbate the the non-linear effects. Consider a pair of satellite galaxies oriented perpendicularly to the line of sight with a separation of $2\,h^{-1}$ Mpc. Assuming they orbit the centre of mass of their dark matter halo at 500 km s^{-1}, we would interpret their physical separation to be greater than $10\,h^{-1}$ Mpc. Thus, in redshift space, FoG effects project non-linear clustering to larger scales, and the magnitude of this effect should be largest for faint red galaxies. By ignoring pairs close to the line of sight, FoG effects mean that satellite pairs with apparent large separations are preferentially removed. However, these pairs do not truly have large separations, and should not contribute to the true large-scale clustering. This explains why removing these pairs brings the results closer in amplitude to the projected clustering results. Given that studies such as Li et al. (2006) have found that the pairwise-velocity-dispersion is greatest for red galaxies with $M_r < -19$, the FoG effect has its strongest impact on the clustering we measure for the faintest galaxies.

Previous studies have found an upturn in the large-scale bias of red galaxies towards faint luminosities, and this behaviour has been attributed to the fact that these galaxies are predominantly satellites in larger-mass haloes (Blanton et al. 2005; Swanson et al. 2008; Cresswell & Percival 2009). In Section 1 we partially motivated this work by pointing out that the implications of Masjedi et al. (2008) and Wang et al. (2009) suggested a possible tension with the previous clustering studies. The results we present in this paper show that the reports of an upturn in the bias relationship likely cannot be interpreted as an upturn in the linear bias, due to systematic effects. We find that the large-scale, linear, bias of red galaxies monotonically decreases with decreasing luminosity. This in turn suggests that satellite faint red galaxies, residing in massive haloes, are not dominant by number with respect to central faint red galaxies or faint red satellites of $\sim L*$ galaxies.

Measurements of the satellite fraction in the red cloud vary. Tinker & Wetzel (2010) suggest a value of 30 per cent which does not vary significantly between $z = 0.4$ and 2. Brown et al. (2008) find that the fraction of stellar mass in satellites increases with host dark matter halo mass – and such that in haloes with $M_{\rm h} > 10^{14}\,{\rm M}_{\odot}\,h^{-1}$ there is more mass in satellites than centrals. At z = 0, they conclude that 30 per cent of the stellar mass in the red sequence (not number of galaxies) is in satellites. Wang et al. (2009), using a group catalogue and studying very faint (dwarf) red galaxies, conclude that at only around 45 per cent are satellites.

Zehavi et al. (2010) suggest an incredibly large satellite fraction of 90 per cent at the faintest end ($-19 < M_r < -20$), up from 33 per cent at the intermediate luminosity range ($-21 < M_r < -20$). Interestingly, the halo occupation distribution (HOD) model that gives these values (driven by the small-scale clustering) overpredicts the large-scale clustering amplitude. An alternative HOD model, that only allows red satellites in haloes with $M_{\rm h} > 10^{13}\,{\rm M}_{\odot}\,h^{-1}$, reduces the total satellite fraction in the red cloud to 34 per cent and provides a significantly better fit to the data at large scales. Note the apparent contradiction to previous studies; forcing satellite red galaxies to only occupy high mass haloes *reduces* the large-scale bias, due to the fact that such a model allows a lower satellite fraction. Combined, the results of previous studies suggest that the satellite fraction of red cloud galaxies is 35 per cent and may increase towards the faint end. This suggests that, while the satellite fraction allows the bias of red galaxies to remain high relative to blue galaxies, the propensity of faint red galaxies to be central galaxies in low-mass haloes allows their bias to decrease monotonically.

Central faint red galaxies present an interesting puzzle in galaxy formation. It has been observationally established that the satellite population is in general redder that central galaxies of the same mass (see, e.g. van den Bosch et al. 2008; Yang, Mo & van den Bosch 2008; Guo et al. 2010). This can be explained by environmental effects as the galaxy falls on to a more massive halo: a slow or a sudden stripping of the gas reservoir, due to infall, ram-pressure or tidal heating (see, e.g. Gunn & Gott 1972; Larson et al. 1980; Moore et al. 1996; Balogh & Morris 2000). However, a central galaxy has not experienced a direct infall on to a larger halo. One possibility is that put forward by Wang et al. (2009), in which galaxies may experience some form of these environmental effects when passing by a dark matter halo (within three times the virial radius), without falling in. Another possibility is simply that the process that shut down star formation in these galaxies in different, or driven by feedback effects.

8 SUMMARY AND CONCLUSIONS

We have computed the large-scale bias of red galaxies in the SDSS DR7 as a function of luminosity. We use both photometric and spectroscopic data to obtain robust results and utilize the largest volume possible. Our major findings are as follows.

(i) The bias of red galaxies we measure in our photometric data implies the faintest red galaxies have the lowest bias (see Fig. 3). This result is independent of any treatment we apply to the data or its analysis.

(ii) The bias increases dramatically with increasing luminosity for galaxies with $M_r < -21$. There is no evidence for evolution in the bias for galaxies with $-19 > M_r > -21$, and there is weak evidence for a decrease in bias with decreasing luminosity for fainter galaxies (see Figs 5, 6 and 7).

(iii) The bias of red galaxies measured in our spectroscopic samples depends greatly on how we choose to analyse the data (see Figs 5 and 6). The treatment that we believe is most free of systematics ($r_{\rm min} > 12\,h^{-1}$ Mpc, $\mu_{\rm max} < 0.5$) recovers a monotonic increase in the bias of red galaxies as a function of luminosity. This suggests that previous reports of an upturn at low luminosities in the large-scale bias red galaxies were systematically affected by a combination of RSD and non-linearities.

The results that we show here, based on the large-scale clustering, give only an incomplete picture of what is happening at the faint end as we cannot disentangle the contribution from central and satellite galaxies to the overall observed bias value. In some sense the bias of faint red galaxies represents the interplay between the number of satellites (with strong bias, in high-mass haloes), and centrals (with low bias, in low-mass haloes). None the less our results are in good qualitative agreement with other measurements of the fraction of red satellites in the sense that the fraction of satellites is not expected to be dominant even at the faint end. Treatment of the clustering of red galaxies utilizing halo-occupation-distribution modelling to constrain the evolution and mass assembly of red galaxies will be presented in a follow-up paper.

ACKNOWLEDGMENTS

We acknowledge Molly Swanson, Zheng Zheng and Peder Norberg for helpful comments and discussions. We acknowledge an anonymous referee for useful comments.

© 2011 The Authors
Monthly Notices of the Royal Astronomical Society © 2011 RAS

AJR and WJP thank the UK Science and Technology Facilities Council for financial support; RT and WJP are also grateful to the Leverhulme trust and the European Research Council.

Funding for the creation and distribution of the SDSS Archive has been provided by the Alfred P. Sloan Foundation, the Participating Institutions, the National Aeronautics and Space Administration, the National Science Foundation, the US Department of Energy, the Japanese Monbukagakusho and the Max Planck Society. The SDSS Web site is http://www.sdss.org/.

The SDSS is managed by the Astrophysical Research Consortium (ARC) for the Participating Institutions. The Participating Institutions are University of Chicago, Fermilab, Institute for Advanced Study, the Japan Participation Group, Johns Hopkins University, the Korean Scientist Group, Los Alamos National Laboratory, Max Planck Institute for Astronomy (MPIA), Max Planck Institute for Astrophysics (MPA), New Mexico State University, University of Pittsburgh, University of Portsmouth, Princeton University, United States Naval Observatory and University of Washington.

REFERENCES

Abazajian K. N. et al., 2009, ApJS, 182, 543
Ball N. M., Loveday J., Brunner R. J., 2008, MNRAS, 383, 907
Balogh M. L., Morris S. L., 2000, MNRAS, 318, 703
Bardeen J. M., Bond J. R., Kaiser N., Szalay A. S., 1986, ApJ, 304, 15
Bell E. F. et al., 2004, ApJ, 608, 752
Blanton M. R. et al., 2003, ApJ, 594, 186
Blanton M. R., Eisenstein D., Hogg D. W., Schlegel D. J., Brinkmann J., 2005, ApJ, 629, 143
Brown M. J. I. et al., 2008, ApJ, 682, 937
Budavári T. et al., 2003, ApJ, 595, 59
Coil A. L., Newman J. A., Cooper M. C., Davis M., Faber S. M., Koo D. C., Willmer C. N. A., 2006, ApJ, 644, 671
Cole S., Kaiser N., 1989, MNRAS, 237, 1127
Conroy C., Ho S., White M., 2007, MNRAS, 379, 1491
Cowie L. L., Songaila A., Hu E. M., Cohen J. G., 1996, AJ, 112, 839
Cresswell J. G., Percival W. J., 2009, MNRAS, 392, 682
Croton D. J., Norberg P., Gaztañaga E., Baugh C. M., 2006, MNRAS, 379, 1562
Dressler A., 1980, ApJ, 236, 351
Eisenstein D. J., Hu W., 1998, ApJ, 496, 605
Feldman H. A., Kaiser N., Peacock J. A., 1994, ApJ, 426, 23
Fukugita M., Ichikawa T., Gunn J. E., Doi M., Shimasaku K., Schneider D. P., 1996, AJ, 111, 1748
Górski K. M., Hivon E., Banday A. J., Wandelt B. D., Hansen F. K., Reinecke M., Bartelmann M., 2005, ApJ, 622, 759
Gunn J. E., Gott J. R., III, 1972, ApJ, 176, 1
Gunn J. E. et al., 1998, AJ, 116, 3040
Guo Q., White S., Li C., Boylan-Kolchin M., 2010, MNRAS, 404, 1111
Haines C. P., Gargiulo A., La Barbera F., Mercurio A., Merluzzi P., Busarello G., 2007, MNRAS, 381, 7
Hamilton A. J. S., 1992, ApJ, 385, L5
Hogg D. W. et al., 2003, ApJ, 585, L5
Jackson J. P., 1972, PhD thesis, The Naval Postgraduate School, Monterey
Jennings E., Baugh C. M., Pascoli S., 2011, MNRAS, 410, 2081
Landy S. D., Szalay A. S., 1993, ApJ, 412, 64
Larson R. B., Tinsley B. M., Caldwell C. N., 1980, ApJ, 237, 692
Li C., Kauffmann G., Jing Y. P., White S. D. M., Borner G., Cheng F. Z., 2006, MNRAS, 368, 21
Madgwick D. S. et al., 2003, MNRAS, 344, 847
Masjedi M., Hogg D. W., Blanton M. R., 2008, ApJ, 679, 260
McCracken H. J. et al., 2007, ApJS, 172, 314
McCracken H. J., Ilbert O., Mellier Y., Bertin E., Guzzo L., Arnouts S., Le Fèvre O., Zamorani G., 2008, A&A, 479, 321
Moore B., Katz N., Lake G., Dressler A., Oemler A., 1996, Nat, 379, 613
Myers A. D., Brunner R. J., Nichol R. C., Richards G. T., Schneider D. P., Bahcall N. A., 2007, ApJ, 658, 85
Norberg P. et al., 2002, MNRAS, 332, 827
Percival W. J., White M., 2009, MNRAS, 393, 297
Petrosian V., 1976, ApJ, 210, L53
Reid B. A. et al., 2009, MNRAS, 404, 60
Ross A. J., Brunner R. J., Myers A. D., 2007, ApJ, 665, 67 (R07)
Ross A. J., Brunner R. J., 2009, MNRAS, 399, 878
Ross A. J., Percival W. J., Brunner R. J., 2010, MNRAS, 407, 420 (R10)
Scranton R. et al., 2002, ApJ, 579, 48
Skibba R. A. et al., 2009, MNRAS, 399, 966
Smith R. E. et al., 2003, MNRAS, 341, 1311
Swanson M. E. C., Tegmark M., Blanton M., Zehavi I., 2008, MNRAS, 385, 1635
Tegmark M., 1997, Phys. Rev. Lett., 79, 3806
Tinker J. L., Wetzel A. R., 2010, ApJ, 719, 88
Wang Y., Yang X., Mo H. J., van den Bosch F. C., Katz N., Pasquali A., McIntosh D. H., Weinmann S. M., 2009, ApJ, 697, 247
van den Bosch F. C., Aquino D., Yang X., Mo H. J., Pasquali A., McIntosh D. H., Weinmann S. M., Kang X., 2008, MNRAS, 387, 79
White S. D. M., Rees M. J., 1978, MNRAS, 183, 341
White M., Zheng Z., Brown M. J. I., Dey A., Jannuzi B. T., 2007, ApJ, 655, L69
Willmer C. N. A., da Costa L. N., Pellegrini P. S., 1998, AJ, 115, 869
Yang X., Mo H. J., van den Bosch F. C., 2008, ApJ, 676, 248
Zehavi I. et al., 2005, ApJ, 630, 1
Zehavi I. et al., 2010, preprint (arXiv:1005.2413)

This paper has been typeset from a TEX/LATEX file prepared by the author.

© 2011 The Authors
Monthly Notices of the Royal Astronomical Society © 2011 RAS